75th International Astronautical Congress (IAC), Milan, Italy, 14-18 October 2024.

IAC–24–C1.9.5

Investigation of Interior Mean Motion Resonances and Heteroclinic Connections in the Earth-Moon System

Bhanu Kumar[a*], **Anjali Rawat**[b], **Aaron J. Rosengren**[c], **Shane D. Ross**[d]

[a] *Jet Propulsion Laboratory, California Institute of Technology, 4800 Oak Grove Drive, Pasadena, CA, USA 91109, bhanu.s.kumar@jpl.nasa.gov*
[b] *Aerospace and Ocean Engineering, Virginia Tech, 495 Old Turner St, Blacksburg, VA, USA 24061, anjalirawat@vt.edu*
[c] *Mechanical and Aerospace Engineering, University of California San Diego, 9500 Gilman Dr, La Jolla, CA, USA 92093, arosengren@ucsd.edu*
[d] *Aerospace and Ocean Engineering, Virginia Tech, 495 Old Turner St, Blacksburg, VA, USA 24061, sdross@vt.edu*
[*] *Corresponding author*

Abstract

Understanding the dynamical structure of cislunar space beyond geosynchronous orbit is of significant importance for lunar exploration, as well as for design of high Earth-orbiting mission trajectories in other contexts. A key aspect of these dynamics is the presence of mean motion resonances, as heteroclinic connections between unstable resonant orbits are fundamental to changing and understanding the evolution over time of a spacecraft's semimajor axis. In this paper, we first compute and analyze several important resonant orbit families within the Earth-Moon system based on the planar circular restricted 3-body problem. Focusing on interior resonances 4:1, 3:1, and 2:1, we identify a number of bifurcations of these resonances' periodic orbit families. Once the aforementioned orbits are computed, we then compute their stable and unstable manifolds using an osculating orbit perigee Poincaré map. Carrying out these computations across a range of energy values, we are able to characterize the range of naturally attainable semimajor axis values for future distant Earth-bound or lunar spacecraft missions.

1. Introduction

In recent years, there has been a rapid and sustained increase in current as well as future planned activities in cislunar space. This includes human lunar spaceflight programs such as NASA's Artemis and Lunar Gateway, as well as robotic lunar exploration missions such as NASA's Lunar Trailblazer and CADRE, the various NASA-sponsored Commercial Lunar Payload Services programs, the Chinese CNSA's Chang'e series of missions. ISRO's Chandrayaan missions, and JAXA's SLIM lander. However, in addition to explicitly Moon-focused exploration missions, the realm of cislunar space has also captured significant interest from other points of view. In 2022, the US White House released its National Cislunar Science and Technology Strategy [1] which explicitly identified space situational awareness in the cislunar domain as a priority area for development. And furthermore, even spacecraft whose missions are completely non Moon-focused may operate in regions of cislunar space where the effects of lunar gravity are significant enough to cause major orbital changes. This must hence be taken into account during the mission design. For instance, during its initial 2-year nominal mission, NASA's Interstellar Boundary Explorer (IBEX) spacecraft was placed into an orbit whose evolution was found to be chaotic and unpredictable beyond 2.5 years due to lunar perturbations. Thus, for its extended mission, IBEX was maneuvered into a stable 3:1 resonant orbit with the Moon [2].

Given the previous discussion, understanding the dynamical structure of cislunar space beyond geosynchronous orbit is of significant importance for both lunar exploration and for design of high Earth-orbiting mission trajectories in other contexts. A key aspect of these dynamics is the presence of mean motion resonances. A number of prior spacecraft have been placed into stable lunar resonant orbits, such as the aforementioned IBEX mission as well as NASA's Transiting Exoplanet Survey Satellite (TESS) [3], while some seemingly orbit in the unstable resonance regime (e.g. Russia's Spektr-R). Although libration point orbits have been studied extensively in the Earth-Moon system (e.g. the book of Simo et al [4]) the intricate nature of mean motion resonances, especially their stable and unstable orbit families and their overlapping heteroclinic connections, is much less explored. A spacecraft following a heteroclinic connection will naturally change its semimajor axis due to the subtle influence of the Moon, without use of propulsion. The presence of such paths can be used beneficially for trajectory design, but could also be potentially hazardous if unanticipated in mission planning.

While heteroclinic connections between resonances [5] are fundamental to changing and understanding the

evolution of a spacecraft's semimajor axis, and have been investigated for trajectory design in the Jovian [6–8] and Saturnian [9] systems, they remain woefully understudied in the Earth-Moon case. In this study, we present two primary contributions: first, we compute and analyze several important resonant orbit families in the Earth-Moon system within the framework of a planar circular restricted 3-body problem model. In this case, unstable resonant orbits are periodic and occur in 1-parameter families. Focusing on interior resonances 4:1, 3:1, and 2:1, we identify a number of bifurcations of these resonances' periodic orbit families. We find and describe relationships between unstable and stable prograde and retrograde resonant orbits. Then, once the aforementioned resonant orbits are computed, we compute their stable and unstable manifolds. This is done using a parameterization method [10] combined with a Poincaré map at osculating orbit perigee. Carrying out these computations across a range of restricted three-body energy values (Jacobi constants) in the Earth-Moon system, we are able to characterize the range of naturally attainable semimajor axis values for future distant Earth-bound or lunar spacecraft missions.

In this paper, we start by briefly reviewing the restricted 3-body model we use as well as some background on resonant orbits and resonance overlapping in Section 2. We then give a brief overview of the computational and visualization methodologies used in this study in Section 3. Next, we describe the interior resonant orbit families computed in the Earth-Moon system. Finally, after using the unstable resonant orbit families computed in the previous step to find their stable and unstable manifolds, we present the heteroclinic connections generated by these manifolds at varying energy levels, and discuss the resulting implications for zero-cost, fully ballistic cislunar trajectory design.

2. Background

2.1 Planar Circular Restricted 3-Body Problem

For completeness, we include the following description of the well-known planar circular restricted 3-body problem (PCRTBP) as reproduced from Kumar et al. [11]. The PCRTBP describes the motion of an infinitesimally small particle (thought of as a spacecraft) under the gravitational influence of two large bodies of masses m_1 and m_2, which revolve about their barycenter in a circular Keplerian orbit (e.g. a planet and a moon). Units are also normalized so that the distance between m_1 and m_2 becomes 1, their period of revolution becomes 2π, and $\mathcal{G}(m_1+m_2)$ becomes 1. We define a mass ratio $\mu = \frac{m_2}{m_1+m_2}$, and use a synodic, rotating non-inertial Cartesian coordinate system centered at the m_1-m_2 barycenter such that m_1 and m_2 are always on the x-axis. In the planar CRTBP, we also assume that the spacecraft moves in the same plane as m_1 and m_2. In this case, the equations of motion are Hamiltonian with form [12]

$$\dot{x} = \frac{\partial H}{\partial p_x} \quad \dot{y} = \frac{\partial H}{\partial p_y} \qquad \dot{p}_x = -\frac{\partial H}{\partial x} \quad \dot{p}_y = -\frac{\partial H}{\partial y} \tag{1}$$

$$H(x, y, p_x, p_y) = \frac{p_x^2 + p_y^2}{2} + p_x y - p_y x - \frac{1-\mu}{r_1} - \frac{\mu}{r_2} \tag{2}$$

where $r_1 = \sqrt{(x+\mu)^2 + y^2}$ is the distance from the spacecraft to m_1 and $r_2 = \sqrt{(x-1+\mu)^2 + y^2}$ is the distance to m_2. For m_1-m_2 as Earth-Moon, respectively, we use $\mu = 1.2150584270572 \times 10^{-2}$. The momenta p_x, p_y are the spacecraft velocity components in an inertial reference frame; they are related to the synodic (non-inertial) frame velocities $\dot{x}, \dot{y}$ as $\dot{x} = p_x + y$, $\dot{y} = p_y - x$.

There are two important properties of Eq. [1]-[2] to note. First of all, the Hamiltonian in Eq. [2] is autonomous and is thus an integral of motion. Hence, PCRTBP trajectories are restricted to 3D energy submanifolds of the state space satisfying $H(x, y, p_x, p_y) =$ constant. The quantity $C = -2H$ is referred to as the *Jacobi constant*, and is generally used in lieu of H to specify energy levels. The second property is that the equations of motion have a time-reversal symmetry. Namely, if $(x(t), y(t), t)$ is a solution of Eq. [1]-[2] for $t > 0$, then $(x(-t), -y(-t), t)$ is a solution for $t < 0$.

2.1.1 Synodic Delaunay coordinates

While Equations [1]-[2] for the PCRTBP are written in Cartesian coordinates, other coordinate systems can also be used to express the Hamiltonian and equations of motion. In certain cases, one of the most beneficial sets of coordinates to use are the *synodic Delaunay coordinates* (L, G, ℓ, g). These coordinates can be most easily defined in terms of the classical (osculating) orbital elements via the equations $L = \sqrt{(1-\mu)a}$, $G = L\sqrt{1-e^2}$, and the definitions $\ell =$ mean anomaly and $g =$ argument of periapse *with respect to the rotating frame positive x-axis*. Note that unlike the traditional argument of periapse, in this case $\dot{g} \approx -1 \neq 0$ as the rotating frame x-axis is constantly moving with respect to an inertial frame.

The main benefits of using synodic Delaunay coordinates stem from the fact that they are action-angle coordinates [12] for the $\mu = 0$ PCRTBP (the Kepler problem in a rotating reference frame). What this means is that 1) when $\mu = 0$, the Hamiltonian H can be written solely as a function of the actions L and G; and 2) the transformation between Cartesian and synodic Delaunay variables is canonical, i.e. the equations of motion in synodic Delaunay coordinates remain Hamiltonian. Note that the tradi-

tional osculating orbital elements satisfy above fact (1) but not (2). Combined, these two facts imply that when $\mu = 0$, $\dot{L} = \dot{G} = 0$ and both $\dot{\ell}$ and $\dot{g}$ are constants. Furthermore, when $\mu > 0$, the rich existing literature on Hamiltonian perturbation theory of near-integrable systems (e.g. [13]) becomes applicable to the system written in synodic Delaunay variables. Although in this study we still use Cartesian coordinates for most computations, we will use synodic Delaunay variables to help us visualize and then interpret our results in line with perturbation theory.

2.2 Mean motion resonances and resonance overlap

Resonant motions are ubiquitous in celestial systems. Among the most important resonant phenomena, especially for astrodynamics, is that of *mean motion resonance* (MMR). Roughly speaking†, an m:n mean motion resonance is a region of a celestial system's phase space where one body (in our case the spacecraft) makes approximately m revolutions around some large central body (Earth in our case) in the same time that another body (here, the Moon) makes n revolutions around the same central body. For spacecraft-moon MMRs, since this is a relation between orbital periods of two bodies with the second body's period being fixed, the different MMRs correspond to certain spacecraft semimajor axis values, one for each MMR.

In multi-body celestial systems, MMR regions contain both stable and unstable resonant orbits with various topological properties. Of these, the unstable resonant orbits are of special interest for mission design and low-cost orbit transfers, as they possess attached stable and unstable invariant manifolds. If the unstable manifold of an orbit contained in one MMR intersects the stable manifold of an orbit contained in another MMR, then one gets a zero-Δv *heteroclinic* trajectory from the first MMR to the second. This dynamical phenomenon, known as *MMR overlap*, in turn yields a natural change of spacecraft semimajor axis. Owing to Chirikov's overlap criterion [14], overlap of MMRs is the key driver of global transport across phase space in celestial systems, as this overlap also destroys mathematical barriers whose existence would otherwise prevent major changes in semimajor axis. MMR overlap thus determines the semimajor axis values a spacecraft can reach without using fuel.

In the PCRTBP, at each mean motion resonance, families of stable and unstable resonant orbits exist over a range of energy levels. The unstable resonant orbits correspond to 1-parameter families of unstable periodic orbits, where the parameter along the family of orbits can be taken as the Jacobi constant [15]. Thus, except for at fold bifurcation points (where C reaches an extremum along the family), locally there will be one unstable resonant periodic orbit for each Jacobi constant C across some range of C values. For the m:n MMR, the resonant periodic orbits will have periods of *approximately* but not exactly $2\pi n$; the range of periods in fact will vary throughout the family as a function of Jacobi constant. Unstable orbits will encounter the Moon at apogee once every m revolutions.

† More rigorously, MMRs are defined through studying the dynamics of certain combinations of angles derived from osculating orbital elements. See for instance the book [13] of Morbidelli for more details.

3. Computational and Visualization Methodologies

In the PCRTBP, to understand the structure of resonant orbit families and the heteroclinic dynamics induced by the unstable ones, one needs to compute the corresponding periodic orbits as well as their stable/unstable manifolds. In order to inform the computations as well as to aid in visualization and dynamical analysis, an appropriate Poincaré section also needs to be chosen and used. Here, we summarize the methods used for these purposes.

3.1 Periapse Poincaré Map

The PCRTBP is a dynamical system on a 4D phase space (x, y, p_x, p_y) with an integral of motion given by the Jacobi constant C. Thus, any one trajectory will lie entirely within a single energy submanifold of form $\mathcal{M}_C = \{(x, y, p_x, p_y) : -2H(x, y, p_x, p_y) = C\}$, where C is the Jacobi constant of that trajectory. Stable and unstable manifolds of a periodic orbit in $\mathcal{M}_C$ will also belong to $\mathcal{M}_C$, as must any heteroclinic connections to other periodic orbits. Thus, for the dynamical analysis we wish to carry out, one can restrict attention to studying the PCRTBP dynamics within $\mathcal{M}_C$ for a variety of C values.

$\mathcal{M}_C$ is a 3D submanifold, so if one now takes a Poincaré surface of section Σ for the PCRTBP flow inside $\mathcal{M}_C$, then Σ will be 2D. Thus, the dynamics of the resulting Poincaré map will be much easier to study than those of the flow, as 2D map dynamics can be relatively easily visualized. Thus, as is standard in PCRTBP studies (see e.g. [15, 16]), we will follow this approach of studying the Poincaré map dynamics. However, ideally the PCRTBP flow should be transverse (i.e. not tangent) to the chosen Poincaré section at all points of the section, or otherwise have tangencies at as few points as possible. The most commonly used Poincaré sections in the literature (i.e. [15, 16]) are those with fixed x or y, but these sections generally experience many tangencies with unstable resonant periodic orbits' stable/unstable manifolds, leading to discontinuities when the manifolds are plotted on the section for analysis (e.g. [15]).

Given the disadvantages of fixed-x or fixed-y Poincaré sections in the PCRTBP, in this study, we instead will use a perigee (Earth-relative osculating true/mean

anomalies = 0) Poincaré surface of section. Such sections have been used by, e.g., Ross and Scheeres [17] and Howell et al. [18] as well; they have much better transversality to the PCRTBP flow as compared to the aforementioned commonly-used sections, as mean anomaly (usually) is always increasing and thus orbits usually don't experience tangencies to the section. The exception to this is in the region around the Moon where Earth's gravity is no longer the dominant influence on the spacecraft; in this case, the geocentric osculating true/mean anomalies can start decreasing, but for the interior resonant orbits and their stable/unstable manifolds studied here, this is not the primary region of interest since intersections with the perigee section occur away from the Moon.

3.1.1 Identifying crossings of the periapse section

To identify crossings of PCRTBP trajectories with the aforementioned periapse Poincaré surface of section during propagation of orbits, rather than trying to directly detect when the osculating true/mean anomalies become zero, we utilize an alternative approach. In particular, it is known that at perigee and apogee, in an inertial reference frame the geocentric position and velocity vectors become perpendicular so that their dot product is zero. Furthermore, this dot product is positive when $\ell \in (0, \pi)$ and negative for $\ell \in (\pi, 2\pi)$. Thus, if we assume mean anomaly is only increasing, then periapse occurs when this dot product crosses zero in an increasing direction, from negative to positive; apoapse occurs in the opposite case. Thus, to detect periapse crossings and distinguish them from (most) apoapses, we look for when

$$[(x + \mu), y] \cdot [p_x, (p_y + \mu)] \qquad [3]$$

crosses from negative to positive during a trajectory propagation. This can be easily implemented in MATLAB or Julia using those languages Events and Continuous Callbacks functionalities, respectively. Note that the additions of μ to x and p_y in Equation [3] are due to the change from barycentered to Earth-centered coordinates.

In the Kepler problem, where mean anomaly ℓ is always increasing, the above strategy will detect every periapse without any false detections. However, if the assumption of $\dot{\ell} > 0$ is broken, then at times the above test may detect a "false periapse" in the PCRTBP even when true/mean anomaly is in fact π rather than zero. This can occur in particular when (geocentric) ℓ briefly starts decreasing near apoapse, which as mentioned earlier can happen when the trajectory closely approaches the Moon. If $\dot{\ell}$ becomes negative near apoapse, then the trajectory can pass through $\ell = \pi$ from $\ell \in (\pi, 2\pi)$ to $\ell \in (0, \pi)$; in this case the dot product in Equation [3] also crosses from negative to positive, just as it does when ℓ passes through 0 and $\dot{\ell} > 0$. To mitigate these false detections, one simply adds an additional check to the periapse event detection algorithm. Namely, if the previous dot product method detects a potential periapse crossing during propagation, then the mean anomaly ℓ of the resulting state is computed; only if ℓ is very near 0 or 2π is the periapse detection then confirmed and the propagation stopped. Both MATLAB and Julia's event detection capabilities can implement such functionality to decide whether or not to stop a numerical integration based on an additional test.

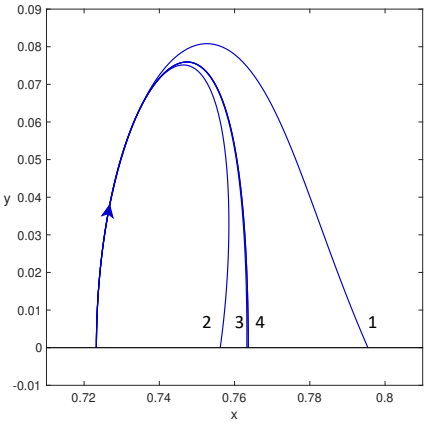

Fig. 1. Illustration of perpendicular x-axis crossings method for computing PCRTBP periodic orbits [20]

3.2 PCRTBP Periodic Orbits

To compute a family of m:n unstable periodic orbits in the Earth-Moon PCRTBP, we start with an orbit state from the Earth Kepler problem having semi-major axis $a = \left(\frac{n}{m}\right)^{2/3}$ and initial argument of periapse and true anomaly both π (for the interior MMRs considered in this study); here, the argument of periapse is measured with respect to the rotating frame positive x-axis. The previously mentioned Keplerian orbit will be symmetric about the x-axis and will also be periodic in the rotating Kepler problem (i.e., PCRTBP with $\mu = 0$). Thus, the method of perpendicular x-axis crossings can be used to numerically continue this Keplerian orbit to the true value of $\mu = 1.2150584270572 \times 10^{-2}$ for the Earth-Moon system; see, for example, Section 2.6.6.2 of Parker and Anderson [19] for details of this method. A schematic illustration of the method is also given in Figure 1. The same method is then used to continue the resulting PCRTBP orbit through the rest of its orbit family, generally using the perpendicular orbit x-intercept as the continuation parameter. Occasionally, when encountering a turning point where this x-intercept reaches an extremum along the family, we instead consider the Jacobi constant C as the pa-

rameter, using an orbit state vs C fit to generate an initial guess for an orbit on the other side of the x-intercept turning point. In this paper, we will consider only symmetric periodic orbits, for which this method is valid.

As a note, an m:n resonant periodic orbit will pass through periapse m times during one orbital period in the PCRTBP. Thus, when using the periapse section described in Section 3.1, the m:n periodic orbit will have m intersection points with the section; moreover, these points will not be fixed points of the section's Poincaré map, but become m-iteration periodic orbits under the map. That is, one will have m points $X(k) \in \Sigma \subset \mathbb{R}^4$, $k = 0, 1, \ldots, m-1$, satisfying the equation

$$P(X(k)) = X(k+1 \mod m) \quad [4]$$

for all k, where $P : \Sigma \to \Sigma$ is the periapse Poincaré map. Furthermore, by definition of the points $X(k)$, there exist times-of-flight $\tau(k) \in \mathbb{R}^+$ such that a trajectory starting at $X(k)$ reaches $X(k+1)$ in time $\tau(k)$ under the PCRTBP flow; in other words, $\tau(k)$ is the first-return time of the point $X(k)$ under the PCRTBP periapse Poincaré map.

3.3 Stable and Unstable Manifolds

Once the periodic orbits in a family m:n have been computed as well as their intersection points $X(k)$ with the periapse section, the computation of the orbits' stable/unstable manifolds is carried out. In particular, we compute the intersection of these manifolds with the periapse section.

The portions of the periodic orbit stable/unstable manifolds lying in the chosen Poincaré section will correspond to 1D curves — one curve for each of the m points of the periodic orbit $X(k)$, $k = 0, 1, \ldots, m-1$ lying in the section. To help accurately compute the manifolds, we extended to the m iteration map-periodic case the first author's previously developed parameterization method [10, 15] for computing Taylor-series approximations of periodic orbit stable/unstable manifolds; this extension also incorporates many methods from the first author's previous work[11] on computing manifolds of invariant tori. Although a full description is beyond the scope of this paper, in short, we solve for a function $W : \{0, \ldots, m-1\} \times \mathbb{R} \to \mathbb{R}^4$ such that for all $k \in \{0, 1, \ldots, m-1\}$

$$\Phi_{\tau(k)}(W(k,s)) = W(k+1 \mod m, \lambda s) \quad [5]$$

where $\Phi_t(\mathbf{x})$ is the PCRTBP flow map of a point $\mathbf{x} \in \mathbb{R}^4$ by time t, $\tau(k)$ are the first return times of the points $X(k)$ as described in Section 3.2, and λ is the mth root of the monodromy matrix eigenvalue corresponding to the stable or unstable manifold. Note that $\Phi_{\tau(k)}(\mathbf{x})$ is *not* the periapse Poincaré mapping P, as the flow propagation time $\tau(k)$ is fixed to the first return time of $X(k)$, not to the return time of the arbitrary point $\mathbf{x} \in \mathbb{R}^4$.

Equation [5] can be solved recursively by expressing W as a set of m Taylor series depending on the integer k

$$W(k,s) = X(k) + \sum_{i=1}^{\infty} W_i(k) s^i \quad k \in \{0, 1, \ldots, m-1\} \quad [6]$$

where $W_1(k) \in \mathbb{R}^4$ are appropriately scaled stable or unstable eigenvectors of the periodic orbit monodromy matrix at each of its periapse passages $X(k)$. The $W_i(k)s^i$ for $i \geq 2$ correspond to higher order (nonlinear) terms in the stable/unstable manifold approximation that are solved recursively. Due to both finite truncation and radius of convergence, these series representations of W will be valid only in a finite radius of validity centered at $s = 0$, which can determined by observing the error in Equation [5] as a function of s; see e.g. [11, 15] for details of similar radius of validity calculations.

As $\Phi_{\tau(k)}(\mathbf{x})$ was not the periapse Poincaré map, the m curves parameterized by W lie near but not on the periapse section of interest Σ. Thus, to finally compute the manifolds on the section, one simply numerically integrates dense grids of points from the domains of validity of those curves either backwards or forwards to the section. Then, further applications of the periapse Poincaré map either forwards or backwards in time are used to respectively globalize the full unstable and stable manifolds. As usual, for each fixed Jacobi constant value C, one can plot these Poincaré map manifolds of various orbits at that C value using just 2D coordinates. Intersections of 1D manifold curves from different orbits on this 2D plot will then give points lying on true heteroclinic trajectories between those orbits. In this study, we use the synodic Delaunay variables (L, g) of Section 2.1.1 as our plotting coordinates.

4. Cislunar Resonant Periodic Orbit Families

As described in Section 2.2, overlap of mean motion resonances allows for natural changes of semimajor axis without use of spacecraft propulsion. This overlap, which corresponds to heteroclinics between unstable resonant orbits, can thus be useful for understanding and designing orbit changes for missions in celestial systems. Thus, a program for determining the extent of such phenomena in cislunar space involves computing the unstable resonant orbits, followed by their stable and unstable manifolds, and finally detecting heteroclinics or barriers to transport between the various resonances in the system. In this section, we describe the first step: the computation of unstable interior resonant orbits, which are periodic in our Earth-Moon PCRTBP model. In addition, to try to gain a more complete understanding of how various resonant periodic orbit families are linked with each other, we will

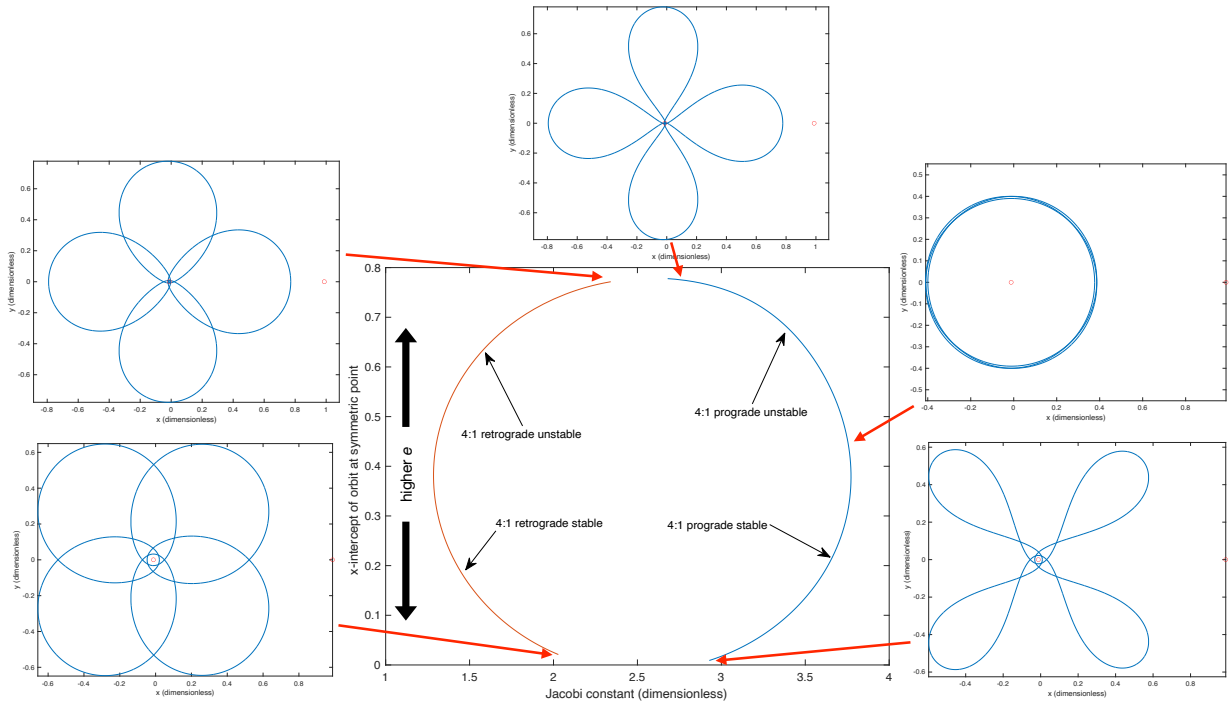

Fig. 2. Bifurcation diagram for 4:1 periodic orbits with example orbit plots (Earth and Moon as red circles)

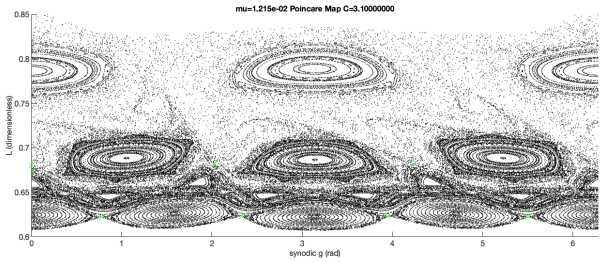

Fig. 3. Poincaré section points for Jacobi C = 3.10

also compute stable resonant periodic orbits.

As described in the introduction, the 2:1 and 3:1 lunar mean motion resonances (MMRs) have been used in prior space missions like TESS and IBEX (albeit both are in stable resonant orbits); thus, we will study these two MMRs. In addition, Poincaré section plots generated by propagating massive number of points to our perigee section also suggested 4:1 as a prominent MMR, which we thus will study as well. For instance, Figure 3 shows such a plot generated for Jacobi constant $C = 3.10$; in this plot, wide stability islands generated by the 2:1 MMR are visible centered near $L = 0.78$, prominent 3:1 islands are visible centered near $L = 0.68$, and also-significant 4:1 islands are clearly visible centered near $L = 0.625$. Note that an m:n MMR displays m "eye" shaped regions in a row at its corresponding value of $L = \sqrt{(1-\mu)a}$.

4.1 Periodic Orbit Families for 4:1 MMR

The 4:1 resonant periodic orbits were computed using the methods of Section 3.2, including stable and unstable periodic orbits. Both prograde and retrograde orbits were computed and numerically continued throughout their families. Figure 2 displays a bifurcation diagram for the resulting orbit families, plotting the perpendicular positive x-axis crossing value of each orbit versus its Jacobi constant, along with a selection of representative orbits. First of all, it should be noted that the unstable and stable prograde 4:1 periodic orbits belong to a single continuous periodic orbit family, so that the stable orbits are continuations of the unstable ones. The same is true of the unstable and stable retrograde 4:1 periodic orbits, which also belong to a single family. The Jacobi constant reaches a maximum or minimum at points where the periodic orbit Floquet multipliers pass through 1, i.e. at a fold bifurcation point, as expected; this marks the dividing point between stable and unstable orbits in each family.

Furthermore, observing the behavior of the x-intercept vs Jacobi C curves at the bottom and top of the bifurcation diagram, it seems likely that in fact the prograde and retrograde orbit families also may connect to each other through yet-to-be-computed orbits having x-intercepts near 0 or 0.8. Such orbits would correspond to collisions or very close approaches with the Earth at periapse (the x-intercepts near 0.8 correspond to apoapse), and were therefore not computed in this study due to numeri-

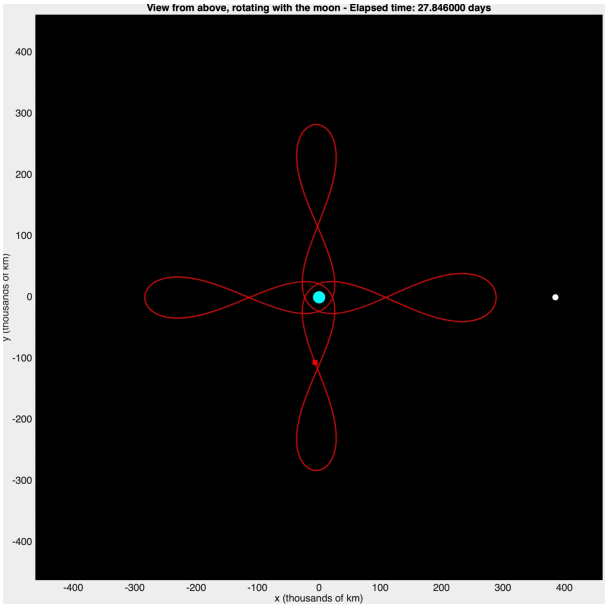

Fig. 4. Example 4:1 unstable resonant orbit

cal difficulties; likely an approach using regularized equations of motion (e.g. that of Levi-Civita [12]) would yield these orbits as well, but we did not implement this yet. Visually comparing the high-eccentricity unstable prograde (top center) and retrograde (top left) orbit plots also suggests that there is likely a continuous family of orbits passing through the Earth singularity joining these two orbits together. Retrograde orbits occur for lower Jacobi constants (higher energies) than the prograde orbits.

The 4:1 orbits range across a wide range of eccentricities, from near-circular (e.g. the top-right unstable orbit plot) to very highly eccentric (the top center orbit plot). An example of a moderate-eccentricity 4:1 unstable orbit is displayed in Figure 4. Finally, note that the semimajor axis of the 4:1 MMR is too small to ever reach at or above the Moon's orbit; even the highest-eccentricity 4:1 orbits, shown in Figure 2, have an apoapse well below the Moon (shown in orbit plots as a red circle at $x = 1 - \mu \approx 1$).

4.2 Periodic Orbit Families for 3:1 MMR

For the 3:1 resonance, again both prograde and retrograde stable and unstable periodic orbits were computed and numerically continued throughout their families. In this case, the stable and unstable orbits are found to belong to separate families, and so we get two separate bifurcation diagrams, one for each family. Figure 5 displays the diagrams for the resulting orbit families, again as a perpendicular x-axis crossing vs Jacobi C plot; the unstable diagram is accompanied by a few unstable periodic orbit plots. In this diagram, note that though each curve corresponding to a prograde/retrograde orbit family crosses a

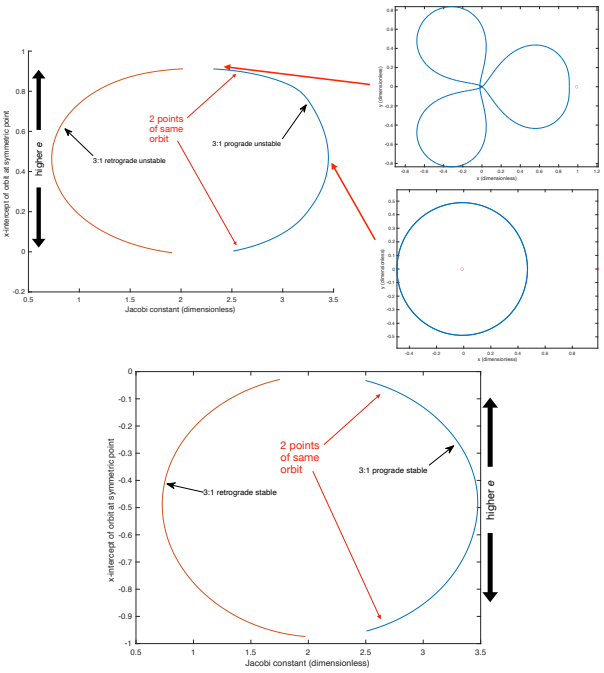

Fig. 5. Bifurcation diagrams for 3:1 unstable (top) and stable (bottom) periodic orbits with example orbit plots (Earth and Moon as red circles)

given Jacobi C twice, both of these crossings correspond to the same orbit; these two replicated portions of a given orbit family both come together at fold bifurcation points where the Floquet multipliers go to 1 and the Jacobi constant reaches a maximum or minimum along the family.

Similar to the 4:1 case described earlier, it is visible from the bifurcation diagrams that the prograde and retrograde unstable orbits are likely in fact connected with each other through a continuous family of orbits passing very near and then through the Earth singularity; the same also is likely true of the stable prograde and retrograde orbits. Again, retrograde orbits occur for lower Jacobi constants/higher energies than prograde orbits. The 3:1 orbits exist over a wide range of eccentricities here as well, from near-circular to highly eccentric, as is displayed for the unstable orbits in the example orbit plots on top right of Figure 5. An example of a moderate-eccentricity 3:1 unstable orbit is displayed in Figure 7. Finally, once again we see that 3:1 unstable orbits never reach at or above the Moon's orbit; even the highest-eccentricity 3:1 unstable orbit shown in top right of Figure 5 has an apoapse well below the Moon (again shown as a red circle at $x = 1 - \mu \approx 1$).

4.3 Periodic Orbit Families for 2:1 MMR

While the 4:1 and 3:1 orbit families in many ways had similar properties, the 2:1 resonant periodic orbit family

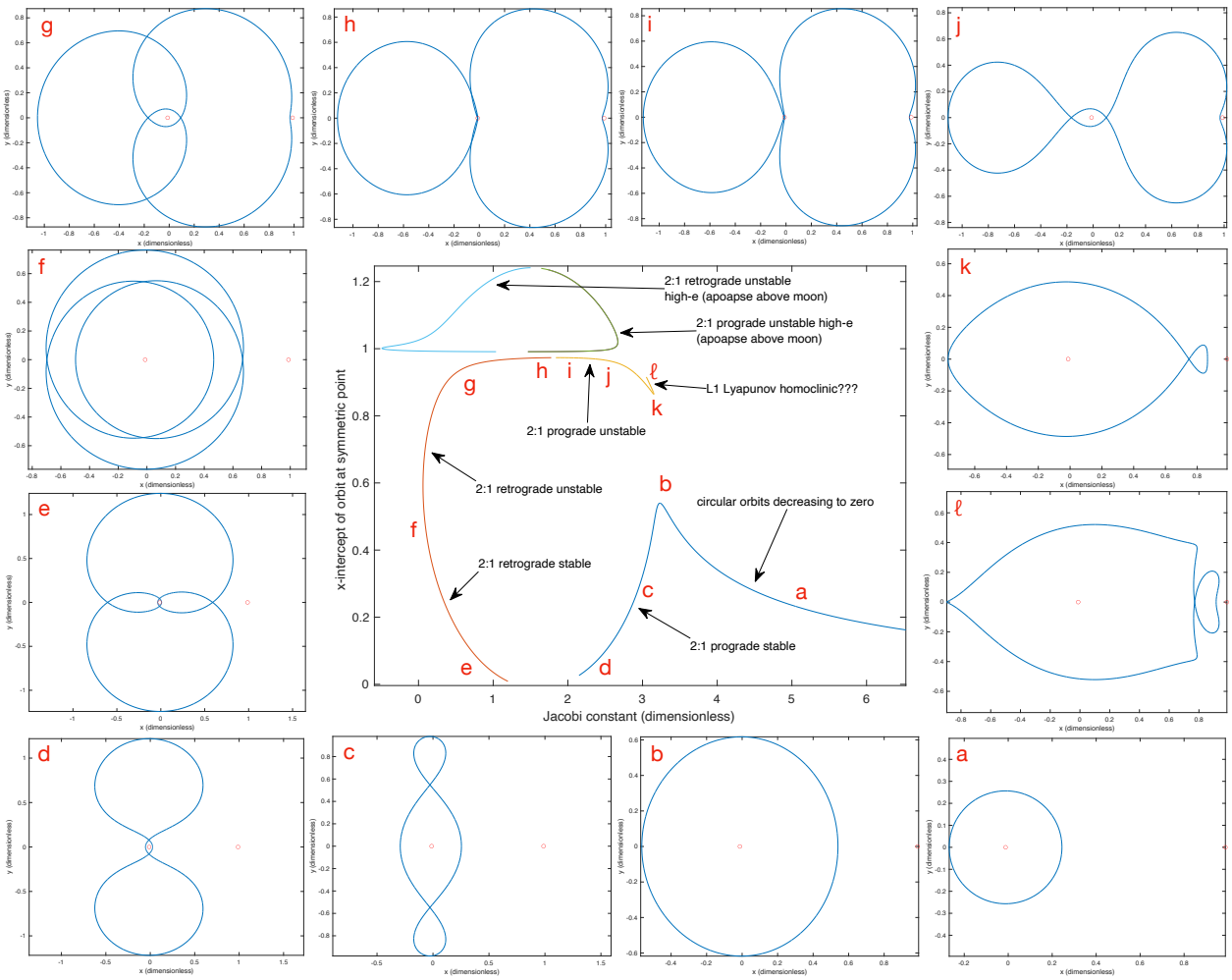

Fig. 6. Bifurcation diagram for orbit family containing 2:1 periodic orbits with example orbit plots (Earth and Moon as red circles)

demonstrates major differences with them in the Earth-Moon PCRTBP. A perpendicular x-axis crossing value vs Jacobi constant C bifurcation diagram for the periodic orbit families containing the 2:1 orbits, similarly constructed to those given earlier for 4:1 and 3:1, is given in Figure 6.

First of all, we discuss the orbits with apoapse below the Moon (x-intercept below $1-\mu$ in Figure 6), examples of which are labeled with letters a-ℓ and plotted in the figure. The orbit family in fact starts with a family of *non-resonant* circular orbits around Earth, with vanishingly small radius as the Jacobi constant goes to infinity; an example of one such circular orbit is orbit (a) of Figure 6. This circular orbit family then *continuously* morphs into the 2:1 stable prograde resonant periodic orbits, which are exemplified by orbits b, c, and d in order of increasing eccentricity and decreasing perigee. It is visible that these stable prograde orbits will then pass through the singularity at Earth and become stable retrograde 2:1 orbits, as also occurred in the 4:1 and 3:1 cases; examples of this are retrograde stable orbits e and f. These retrograde stable orbits then continuously join with retrograde unstable 2:1 orbits, exemplified by g and h, after passing through a fold bifurcation corresponding to a minimum in Jacobi C. It is clear from the bifurcation diagram and orbit plots that the retrograde unstable orbits' periapse will pass through the singularity at Earth again, and will then continuously join with the prograde unstable 2:1 orbits, for example orbits i, j, and k in order of decreasing eccentricity. These orbits eventually encounter another fold bifurcation point where C reaches a local maximum, after which the unstable prograde 2:1 orbits (very briefly) become stable, followed by again becoming unstable and continuously joining a family of *non-resonant* orbits exemplified by orbit ℓ. This last orbit visually seems to be generated by a homoclinic tra-

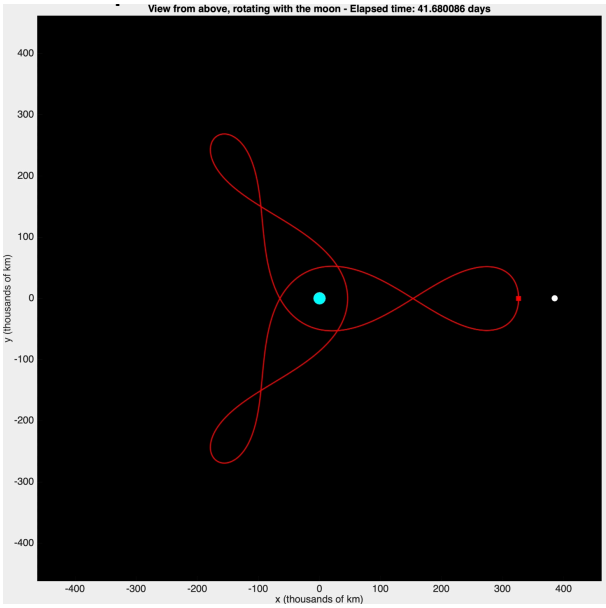

Fig. 7. Example 3:1 unstable resonant orbit

jectory to an L1 planar Lyapunov orbit, although further investigation is needed to confirm this.

Immediately, some key differences with 3:1 and 4:1 orbit families become apparent, First of all, still concentrating on the chain of orbits discussed above, the stable prograde and unstable prograde 2:1 resonant periodic orbit families do not end by joining each other at a fold bifurcation point as occurred in the 4:1 case; instead they continuously connect to families of non-resonant orbits. In the 4:1 case, this fold bifurcation point corresponded to a near-circular low-eccentricity orbit, but in the 2:1 case there is instead a large vertical "gap" between orbits b and k on the plot above. This gap occurs where otherwise one might have expected to find low-eccentricity 2:1 unstable prograde orbits, which we believe do not exist in the Earth-Moon system. Indeed, we also tried continuation by μ of several low-eccentricity 2:1 prograde unstable resonant periodic orbits from the $\mu = 0$ rotating Kepler problem; however, all of these attempts encountered fold bifurcations, where μ would reach a maximum along the curve of continuation solutions and then would start decreasing seemingly to negative infinity, thus never reaching the Moon's μ value. Other non-continuation based methods of searching for periodic orbits directly in the PCRTBP also failed to locate any low-eccentricity 2:1 prograde unstable orbits.

Another major difference between the 2:1 resonant periodic orbits and the 3:1 and 4:1 families discussed earlier is that there are 2:1 orbits whose apoapses go beyond the Moon; these correspond to the prograde and retrograde unstable orbit family curves having x-intercept greater than

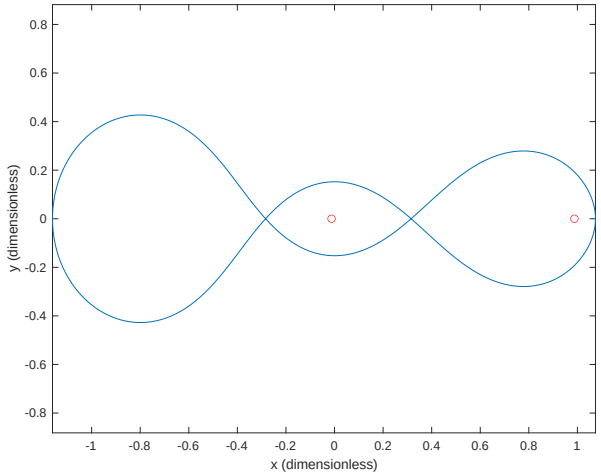

Fig. 8. 2:1 prograde unstable orbit, apoapse above Moon

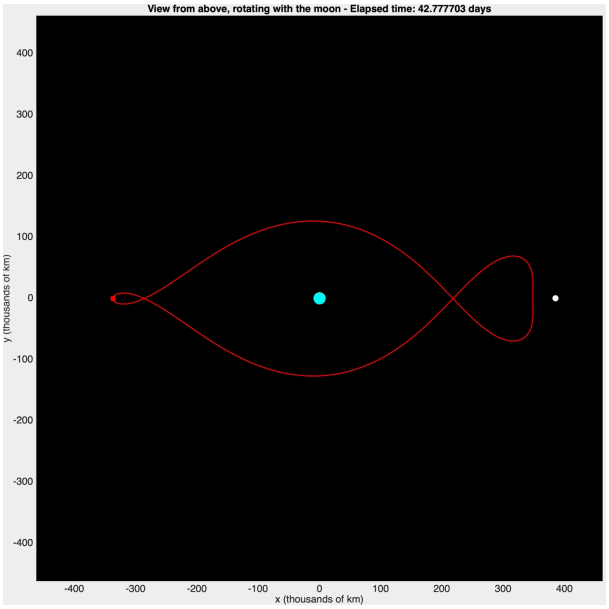

Fig. 9. Example 2:1 unstable resonant orbit

$1 - \mu$ in Figure 6. An example of such an orbit is shown in Figure 8. For these orbits having an apoapse past the Moon, looking at the bifurcation diagram again strongly visually suggests that the retrograde and prograde orbit families will likely join each other continuously after passing through the singularity at Earth.

As a final example, a 2:1 prograde unstable orbit of moderate eccentricity is plotted and shown in Figure 9. We would like to note that the continuous family of orbits joining orbits a through ℓ together in Figure 6 was computed by Broucke [21] in 1968, where he refers to it as "Family BD". They are not identified as belonging to the 2:1 MMR in that work, however, nor are the unstable 2:1

orbits with apoapse above the Moon calculated either.

5. Resonance overlap and natural transport

With the 4:1, 3:1, and 2:1 families of resonant periodic orbits computed and characterized, we are now ready to compute and visualize the unstable resonant orbits' stable and unstable manifolds and search for heteroclinics between them, using the methodology described in Section 3. As a reminder, we plot all manifolds on a perigee Poincaré surface of section, using synodic Delaunay coordinates (g, L) for visualization, where $L = \sqrt{(1-\mu)a}$ and g is the argument of periapse relative to the synodic frame x-axis; we plot L rather than G as orbit size is easier to interpret from L. We will compute manifolds and plot them on the perigee section for a variety of Jacobi constants, starting with a discussion of the 3:1 and 2:1 MMRs and then investigating the 4:1 resonance as well. In this portion of the study, we will analyze only prograde orbits.

5.1 Stable/unstable manifolds of low-energy 3:1 orbits

As described in Section 4.3, the 2:1 unstable prograde resonant orbits only exist for higher eccentricities, which corresponds to higher energies and lower Jacobi constants C. The 3:1 and 4:1 unstable prograde orbits on the other hand existed over a wide range of eccentricities. Indeed, while we found 3:1 unstable orbits even at a Jacobi C of 3.45, the lowest-energy 2:1 unstable orbit found has a Jacobi C of just above 3.15. Thus, there is a significant range of energy values for which 3:1 (and 4:1) unstable orbits exist, but not 2:1 unstable orbits.

First consider this range of Jacobi constants $C \in [3.16, 3.45]$ between the appearance of the 3:1 unstable orbits and the appearance of 2:1 unstable orbits. Computing the manifolds and plotting them on our perigee section as shown in Figure 10, we see that for higher Jacobi constants in that range (the top two plots), the manifolds closely resemble the separatrices of a mathematical pendulum phase portrait. This is what perturbation theory [13] predicts should occur in a region dominated by a single resonance, without overlapping with other resonances. Even as we approach the appearance of the 2:1 orbits at $C = 3.15$, the 3:1 manifolds retain their similarity to pendulum separatrices, except that the homoclinic intersections between stable and unstable 3:1 orbit manifolds become more and more transverse; this is shown in the bottom plot of Figure 10, which is for $C = 3.158$. Note that the top half of the 3:1 orbit manifolds extends significantly further in L than the bottom half for this last C value.

5.2 Heteroclinics between 3:1 and 2:1 orbits

We now turn our attention to the range of Jacobi constants for which both 2:1 and 3:1 unstable periodic orbits

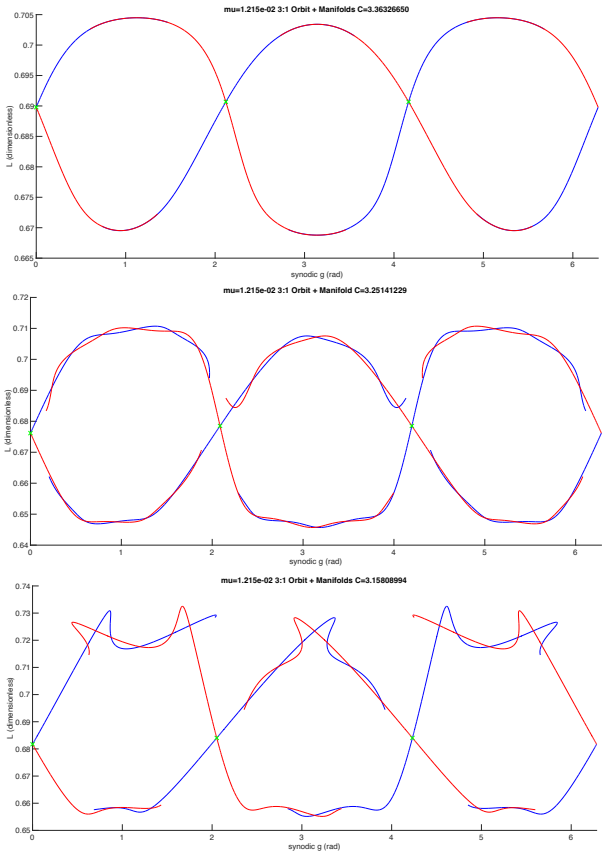

Fig. 10. 3:1 stable/unstable manifolds (blue/red), perigee section, from top to bottom: $C = 3.363, 3.251, 3.158$

exist, that is for $C \leq 3.15$. In Figure 11, we show the computed stable/unstable manifolds of the 3:1 and 2:1 orbits in green/magenta and blue/red, respectively, plotted on our perigee Poincaré section for $C = 3.15, 3.10, 3.05, 3.00$. The grey background points are other non-manifold trajectory points found by propagating massive number of trajectories to our section, similar to the previous Figure 3, and help provide context as to the regions of phase space through which the manifolds generate motions.

In particular, as soon as the 2:1 unstable orbits (and thus their manifolds) appear for Jacobi constants just above 3.15, heteroclinics between the 3:1 and 2:1 orbits are generated. This is visible in the top left plot of Figure 11 which is for $C = 3.15$. This is in contrast to the more standard resonance overlap behaviors observed in systems with lower μ such as Jupiter-Europa, where there is a range of low energies/high C values for which two unstable resonant orbits exist without having any overlap between them; we suspect that this behavior indicates that the 2:1 resonance lies in a region where the standard results from Hamiltonian perturbation theory start to partially break down. As another observation along these

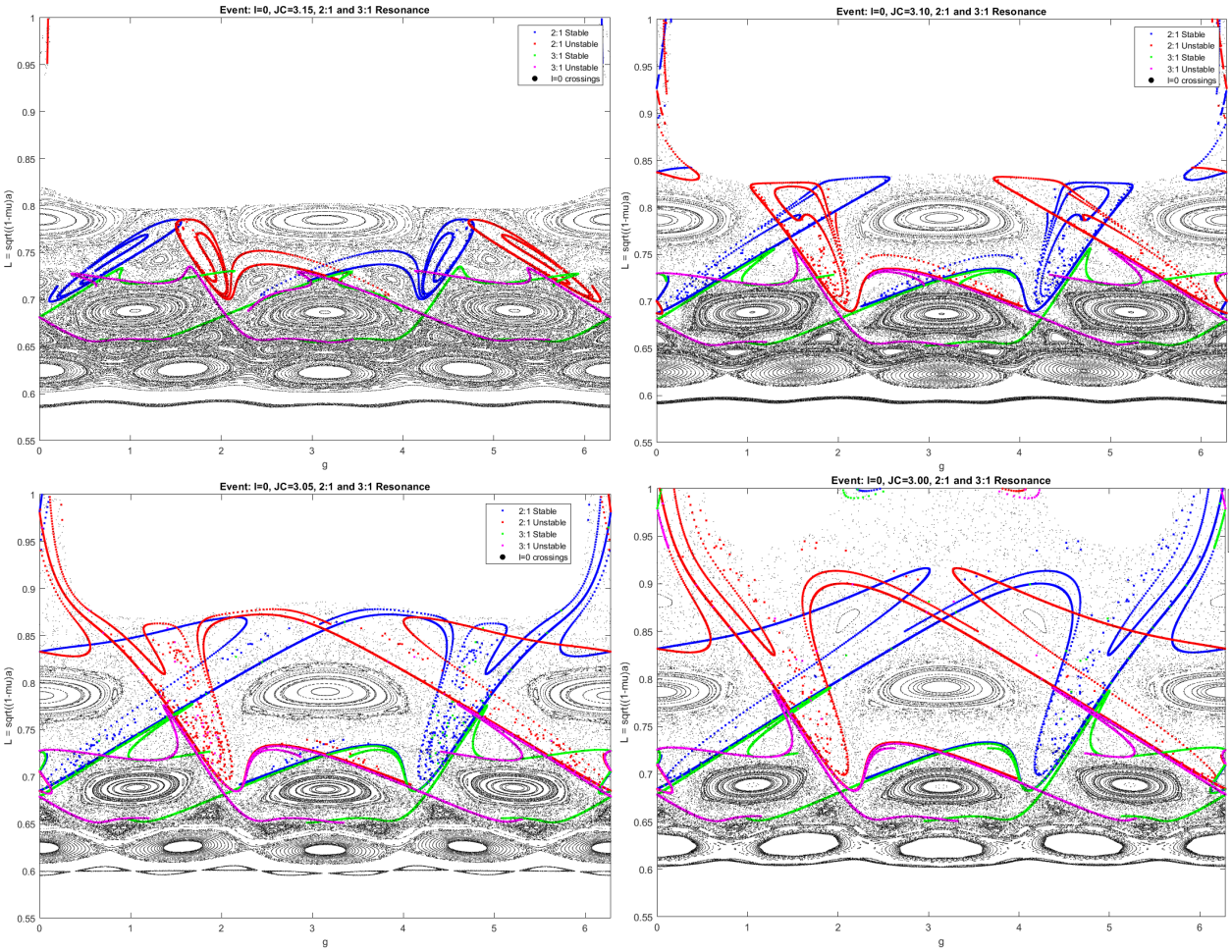

Fig. 11. 3:1 (green/magenta) and 2:1 (blue/red) orbit stable/unstable manifolds on perigee Poincaré sections along with other propagated trajectories in gray, for Jacobi constants $C = 3.15, 3.10, 3.05, 3.00$ (see plot titles for C values)

lines, we see that for both $C = 3.15$ and 3.10 (the top two plots of Figure 11, the top portion (above the center of the 2:1 resonance at $L \approx 0.78$) of the 2:1 manifolds is not at all shaped like a mathematical pendulum; in fact for $C = 3.15$, the top part of the 2:1 stable and unstable manifolds do not even intersect each other except at the 2:1 periodic orbit points themselves. Further investigations [22] have suggested that this unexpected behavior for $C = 3.10$ and 3.15 may be related to tube dynamics induced by manifolds of planar Lyapunov orbits, although further study of these cases is still required.

For all the values of $C \leq 3.15$, we have heterocilnic connections between the 3:1 and 2:1 unstable orbits. For $C = 3.10$ and lower, we observe that several points from the 2:1 orbit manifolds also escape towards $L = 1$, corresponding to the Moon's semimajor axis value; a smaller number of points do the same for $C = 3.15$ as well, though generally the transport towards the Moon becomes stronger for lower Jacobi constants/higher energies as one would expect. For $C = 3.05$ and 3.00, the top part of the 2:1 orbit manifolds finally does also develop a homoclinic intersection, making the manifolds more similar to the typical pendulum separatrix shape than was the case for $C = 3.15$ and 3.10. The overall picture of the manifolds and heteroclinics between them does not change significantly between $C = 3.05$ and 3.00. An example of a 3:1 to 2:1 heteroclinic trajectory for $C = 3.05$ is shown in Figure 12, with the starting 3:1 orbit shown in cyan and destination 2:1 orbit in green.

In summary, for energies $C \leq 3.15$ where 2:1 unstable orbits exist, there exist zero-Δv paths from the 3:1 MMR to 2:1. And for lower Jacobi constants than $C = 3.10$, one can also easily reach the Moon from a 2:1 unstable resonant orbit. Though here we only demonstrated results for $C = 3.00$ to 3.15, the same also holds for lower C [22]. Thus, one can insert into a sufficiently high-energy

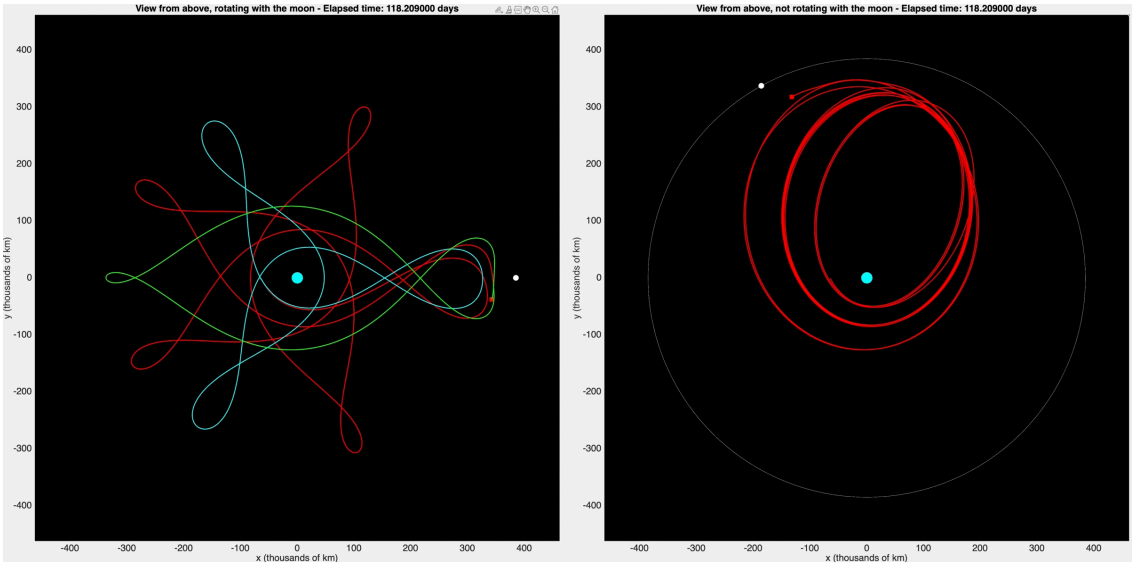

Fig. 12. Example 3:1 to 2:1 heteroclinic transfer for $C = 3.05$, synodic frame on left and inertial frame on right

3:1 orbit's stable manifold, and then surf heteroclinic connections and manifolds to the Moon, which would likely save significant propellant versus a more direct injection.

5.3 The 4:1 resonance and barriers to transport

Having found that it is possible to transfer without Δv from the 3:1 to 2:1 resonances given a sufficiently high energy level, it is natural to ask whether natural transfers from 4:1 to 3:1 may also be possible. If so, then one would be able to start in a 4:1 orbit and follow a chain of heteroclinics until the Moon without using propellant.

In Figure 13, we show stable and unstable manifolds of 4:1 unstable resonant orbits for $C = 3.15, 3.00$, and 2.85 plotted on our perigee Poincaré surface of section. It is immediately visible that these manifolds are shaped very similarly to pendulum phase portrait separatrices, as would be the case in a region dominated by a single resonance without other MMRs overlapping. In fact, for $C = 3.15$ and 3.00, the 4:1 stable and unstable manifolds seem to almost lie on top of each other, very much like the case of an ideal pendulum whose stable/unstable manifolds exactly coincide. This strongly suggests that no heteroclinic can occur from these orbits to the 3:1 MMR or beyond; the same is in fact also visible for the 4:1 orbit at $C = 2.85$, whose stable and unstable manifolds intersect slightly more transversally than those of 3.00 and 3.15, but still clearly do not make significant excursions to other L values. Comparing these 4:1 manifolds to the 3:1 orbit manifolds computed earlier, we are clearly in a situation similar to the top two manifold plots of Figure 10 which had no heteroclinics to 2:1, rather than the case of Figure 11 where heteroclinics first appeared.

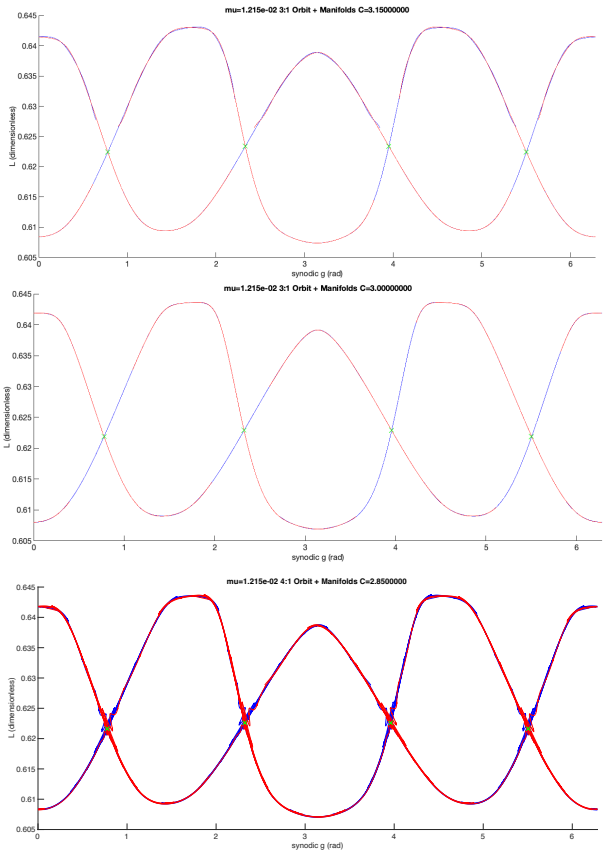

Fig. 13. 4:1 stable/unstable manifolds (blue/red), perigee section, from top to bottom: $C = 3.15, 3.00, 2.85$

The above evidence suggests that the 4:1 orbits for energies $C \geq 2.85$ do not have heteroclinics to the 3:1 MMR

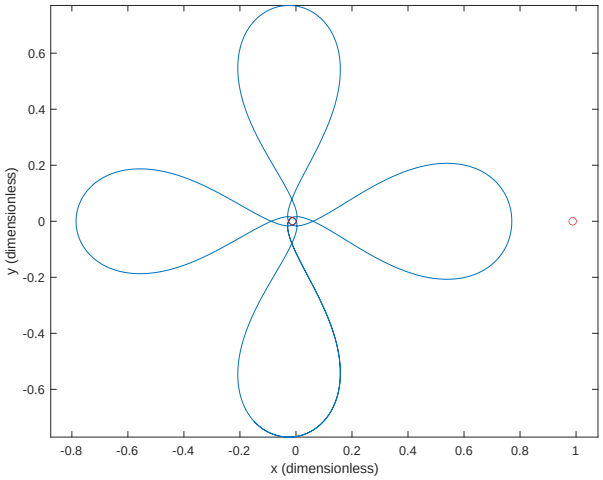

Fig. 14. 4:1 unstable resonant orbit at $C = 2.85$

as one might have hoped. While one might hope that perhaps further decreasing C (increasing energy) might yield a 4:1 orbit with a heteroclinic, the $C = 2.85$ orbit already has such a high energy and eccentricity that its periapse passes below the surface of the Earth, as shown in Figure 14. 4:1 prograde unstable orbits with higher energy and lower C will all have even higher eccentricities than this one and thus will also collide with the surface of the Earth. Even after nevertheless studying such orbits, we still did not detect any heteroclinics between such Earth-collision 4:1 orbits and the 3:1 orbits at such low C values. Overall, we believe that there are no heteroclinic connections from any 4:1 orbit to any 3:1 orbit in the Earth-Moon system.

To understand why no heteroclinics from 4:1 to 3:1 seem to be available, a clue can be seen in the $C = 3.10$ plot of Figure 11. Here, a continuous curve stretching horizontally across the entire plot, from $g = 0$ to 2π, seems to be present just above the 4:1 resonant island (the four "eye" shaped regions centered near $L = 0.625$). This curve seems to be a 1D KAM torus [23], sometimes also referred to in the 2D map case as a rotational invariant circle (RIC) [17], of our PCRTBP Poincaré map; these curves would be formed by Keplerian orbits which persist (after deformation) into the PCRTBP. A key property of such curves is that they form barriers to transport between different resonances, as stable/unstable manifolds cannot intersect them. Thus, this curve is clearly separating the 4:1 and 3:1 MMRs for this Jacobi constant value $C = 3.10$, preventing heteroclinics between them. Although less clear in the figure, a similar curve seems to also potentially exist for $C = 3.05$. For $C = 3.00$ and below, a simple visual identification is not so easy, but we suspect that similar RICs most likely are the barrier preventing heteroclinics from 4:1 to 3:1 orbits from occurring over the entire range of C values considered.

6. Conclusions

In this study, we demonstrated that mean motion resonances play a major role in the dynamical structure of cislunar space. After computing and characterizing families of unstable and stable 4:1, 3:1, and 2:1 resonant periodic orbits, in which the 2:1 family was found to have a very unique and interesting structure, we computed stable and unstable manifolds of the prograde unstable resonant orbits. By using a periapse Poincaré section with synodic Delaunay variables, we were able to effectively visualize the resulting manifolds in a manner that allowed us to identify and interpret the observed phenomena in line with Hamiltonian perturbation theory. Heteroclinics between 2:1 and 3:1 unstable resonant orbits were found to occur for Jacobi constants below 3.15, whereas it was also shown that the 4:1 MMR does not have any natural heteroclinics with the 3:1 MMR for any energy. Hence, we have identified the 3:1 mean motion resonance as truly being a "gateway to the Moon" for lower-energy mission design.

Also in this study, we found that the Earth-Moon PCRTBP resonant orbit and heteroclinic structure can at times vary quite significantly from that of previously-studied systems with much smaller μ values, e.g. outer planet-moon or star-planet CRTBPs, which usually follow perturbation theory-type dynamics fairly closely. Thus, a CRTBP-based analysis of the Earth-Moon system is shown to be crucial to understanding the resonant dynamics of cislunar space. Our additional recent work [22] leveraging the manifolds computed in this study has further demonstrated that a full CRTBP-based analysis of cislunar space is of great import, as comparisons with a perturbed Kepler problem-based semi-analytical approach showed that the latter tends to greatly underestimate the widths and effects of the 2:1 and 3:1 resonances.

While this study as well as [22] both considered only the planar Earth-Moon CRTBP, many spacecraft actually orbit in inclined orbits relative to the Earth-Moon orbital plane. This is in fact the case for the TESS and IBEX spacecraft mentioned earlier which orbit in inclined stable 2:1 and 3:1 resonant orbits. Thus, a generalization of this study to the spatial CRTBP would be the most significant future direction for this research. This will also require the development of new tools to handle the greater dimensionality of the system, as even after reduction to a Poincaré map on an energy submanifold, the spatial CRTBP remains a 4D symplectic map. Apart from the spatial extension, it may also be of interest to investigate the effect of other less significant MMRs such as 5:2 or 7:2. Finally, although it was observed that the unstable manifolds of the 2:1 orbits do lead towards the Moon, a better understand-

ing of heteroclinic connections from 2:1 resonant orbits to L1 Lyapunov orbits would also be of utility for future lunar missions as well as for potentially explaining some of the dynamical behaviors observed in this study.

Acknowledgements

B. Kumar was supported in part by the National Science Foundation (NSF) under a Mathematical Sciences Postdoctoral Research Fellowship award no. DMS-2202994, and in part by the US Air Force Office of Scientific Research (AFOSR) under Award No. FA8655-24-1-7012. This research was carried out in part at the Jet Propulsion Laboratory, California Institute of Technology, under a contract with the National Aeronautics and Space Administration (80NM0018D0004). A.J. Rosengren and S.D. Ross acknowledge support from the Air Force Office of Scientific Research (AFOSR) under Grant No. FA9550-24-1-0194.

References

[1] National Science and Technology Council, *National cislunar science and technology strategy*, Nov. 2022. [Online]. Available: https://www.whitehouse.gov/wp-content/uploads/2022/11/11-2022-NSTC-National-Cislunar-ST-Strategy.pdf.

[2] J. Carrico *et al.*, "Lunar-resonant trajectory design for the Interstellar Boundary Explorer (IBEX) extended mission," *Advances in the Astronautical Sciences*, vol. 142, pp. 771–789, Jan. 2012.

[3] D. J. Dichmann, J. J. Parker, C. Nickel, and S. Lutz, "Trajectory design to mitigate risk for the Transiting Exoplanet Survey Satellite (TESS)," in *AIAA/AAS Astrodynamics Specialist Conference*. DOI: 10.2514/6.2016-5664. eprint: https://arc.aiaa.org/doi/pdf/10.2514/6.2016-5664. [Online]. Available: https://arc.aiaa.org/doi/abs/10.2514/6.2016-5664.

[4] G. Gómez, J. Llibre, R. Martínez, and C. Simó, *Dynamics and Mission Design Near Libration Points*, 4 vols. Roma: World Scientific, 2001.

[5] W. S. Koon, M. W. Lo, J. E. Marsden, and S. D. Ross, "Heteroclinic connections between periodic orbits and resonance transitions in celestial mechanics," *Chaos: An Interdisciplinary Journal of Nonlinear Science*, vol. 10, no. 2, pp. 427–469, 2000. DOI: 10.1063/1.166509. eprint: https://doi.org/10.1063/1.166509. [Online]. Available: https://doi.org/10.1063/1.166509.

[6] R. L. Anderson and M. W. Lo, "Dynamical systems analysis of planetary flybys and approach: Planar Europa orbiter," *Journal of Guidance, Control, and Dynamics*, vol. 33, no. 6, pp. 1899–1912, 2010. DOI: 10.2514/1.45060. eprint: https://doi.org/10.2514/1.45060. [Online]. Available: https://doi.org/10.2514/1.45060.

[7] R. Anderson and M. Lo, "A dynamical systems analysis of resonant flybys: Ballistic case," *The Journal of the Astronautical Sciences*, vol. 58, Apr. 2011. DOI: 10.1007/BF03321164.

[8] R. L. Anderson, S. Campagnola, D. Koh, T. P. McElrath, and R. M. Woollands, "Endgame design for Europa Lander: Ganymede to Europa approach," *The Journal of the Astronautical Sciences*, vol. 68, no. 1, pp. 96–119, 2021. DOI: 10.1007/s40295-021-00250-7. [Online]. Available: https://doi.org/10.1007/s40295-021-00250-7.

[9] M. Vaquero Escribano, "Spacecraft transfer trajectory design exploiting resonant orbits in multi-body environments," Ph.D. dissertation, Purdue University, 2013.

[10] À. Haro, M. Canadell, J. Figueras, A. Luque, and J. Mondelo, *The Parameterization Method for Invariant Manifolds: From Rigorous Results to Effective Computations* (Applied Mathematical Sciences). Springer International Publishing, 2016, vol. 195, ISBN: 9783319296623.

[11] B. Kumar, R. L. Anderson, and R. de la Llave, "Rapid and accurate methods for computing whiskered tori and their manifolds in periodically perturbed planar circular restricted 3-body problems," *Celestial Mechanics and Dynamical Astronomy*, vol. 134, no. 1, p. 3, 2022. DOI: 10.1007/s10569-021-10057-1. [Online]. Available: https://doi.org/10.1007/s10569-021-10057-1.

[12] A. Celletti, *Stability and Chaos in Celestial Mechanics* (Astronomy and Planetary Sciences). Springer-Verlag Berlin Heidelberg, Jan. 2010. DOI: 10.1007/978-3-540-85146-2.

[13] A. Morbidelli, *Modern celestial mechanics : aspects of solar system dynamics*. London: Taylor & Francis, 2002.

[14] B. V. Chirikov, "Resonance processes in magnetic traps," *The Soviet Journal of Atomic Energy*, vol. 6, no. 6, pp. 464–470, 1960. DOI: 10.1007/BF01483352. [Online]. Available: https://doi.org/10.1007/BF01483352.

[15] B. Kumar, R. L. Anderson, and R. de la Llave, "High-order resonant orbit manifold expansions for mission design in the planar circular restricted 3-body problem," *Communications in Nonlinear Science and Numerical Simulation*, vol. 97, p. 105 691, 2021, ISSN: 1007-5704. DOI: https://doi.org/10.1016/j.cnsns.2021.105691. [Online]. Available: http://www.sciencedirect.com/science/article/pii/S1007570421000022.

[16] W. S. Koon, M. W. Lo, J. E. Marsden, and S. D. Ross, *Dynamical systems, the three-body problem and space mission design*. Marsden Books, 2011. [Online]. Available: http://www.dept.aoe.vt.edu/~sdross/books/KoLoMaRo_DMissionBook_2011-04-25.pdf.

[17] S. D. Ross and D. J. Scheeres, "Multiple gravity assists, capture, and escape in the restricted three-body problem," *SIAM Journal on Applied Dynamical Systems*, vol. 6, no. 3, pp. 576–596, 2007. DOI: 10.1137/060663374. eprint: https://doi.org/10.1137/060663374. [Online]. Available: https://doi.org/10.1137/060663374.

[18] K. C. Howell, D. C. Davis, and A. F. Haapala, "Application of periapse maps for the design of trajectories near the smaller primary in multi-body regimes," *Mathematical Problems in Engineering*, vol. 2012, no. 1, p. 351 759, 2012. DOI: https://doi.org/10.1155/2012/351759. eprint: https://onlinelibrary.wiley.com/doi/pdf/10.1155/2012/351759. [Online]. Available: https://onlinelibrary.wiley.com/doi/abs/10.1155/2012/351759.

[19] J. S. Parker and R. L. Anderson, *Low-Energy Lunar Trajectory Design* (JPL Deep Space Communications and Navigation Series), 1st. Hoboken, New Jersey: John Wiley & Sons, Inc., Jun. 2014, vol. 12.

[20] R. L. Anderson, Personal communication, Apr. 2024.

[21] R. Broucke, "Periodic orbits in the restricted three-body problem with earth-moon masses," Tech. Rep. 32-1168, 1968.

[22] A. Rawat, B. Kumar, A. J. Rosengren, and S. D. Ross, "Resonance widths, chaotic zones, and transport in cislunar space," in *AAS/AIAA Astrodynamics Specialist Conference*, Aug. 2024.

[23] R. De la Llave, "A tutorial on KAM theory," in *Smooth Ergodic Theory and Its Applications, Seattle, WA, 1999*, American Mathematical Society, vol. 69, Providence, RI, 2001, pp. 175–292, ISBN: 9780821826829. DOI: 10.1090/pspum/069/1858536.